

Baryon Stopping and Associated Production of Mesons in Au+Au Collisions at $\sqrt{s_{NN}} = 3.0$ GeV at STAR*

BENJAMIN KIMELMAN (FOR THE STAR COLLABORATION)

University of California, Davis

Received July 28, 2022

In these proceedings, we present the first measurements of identified charged hadrons in Au+Au collisions at $\sqrt{s_{NN}} = 3.0$ GeV. Results of baryon stopping, associated production of kaons, and the Coulomb potential of stopped protons are presented. Physics implications of these measurements are discussed.

1. Introduction

1

2 Relativistic heavy-ion collisions are a prime tool to probe the phase
3 structure of strongly interacting matter under extreme conditions. The
4 RHIC Beam Energy Scan II (BES-II) program has three primary goals:
5 searching for the onset of the Quark-Gluon Plasma (QGP), studying the
6 properties of the produced QCD matter, and locating the possible QCD
7 phase boundary and critical endpoint [1].

8 Particle production has long been used to investigate the properties of
9 the produced QCD matter in heavy-ion collisions. The BES-II program
10 covers a wide range of energies, including the transition from a hadronic
11 dominated medium to a partonic dominated one, which has been predicted
12 to occur around $\sqrt{s_{NN}} = 7.7$ GeV [2]. The BES-II program was designed to
13 improve and extend upon the results from the BES-I program. Of particular
14 interest is the high baryon density region which is accessible through the
15 STAR fixed-target program that extends the energy reach from $\sqrt{s_{NN}} = 7.7$
16 GeV to $\sqrt{s_{NN}} = 3.0$ GeV. In these proceedings, the first measurements of
17 charged particle production in Au + Au collisions at $\sqrt{s_{NN}} = 3.0$ GeV are
18 presented. These data were collected in 2018 and contain 275M minimum-
19 bias events.

* Presented at Quark Matter 2022

20

2. Charged Hadron Spectra

21 Charged hadron spectra are obtained using a combination of data from
 22 the Time Projection Chamber (TPC) and barrel Time of Flight (bTOF).
 23 The specific energy loss (dE/dx) can be obtained from the TPC and the
 24 mass squared (m^2) can be obtained from the bTOF, both of which are
 25 binned in rapidity (y), transverse mass ($m_T - m_0$), and centrality. Each
 26 bin is fit with multiple Gaussian distributions to determine the yield of the
 27 particle of interest while accounting for contamination from other particle
 28 species.

29 Invariant yields are obtained after correcting for the limited detector ac-
 30 ceptance and efficiency, which are obtained by embedding simulated tracks,
 31 after passing through the GEANT simulation of the detector response, into
 32 real data. Pion spectra are fit with a double thermal function in order to
 33 extrapolate to the unmeasured region at low $m_T - m_0$; this same fit function
 34 was used by the E895 experiment to describe the pion production from the
 35 Δ -resonance at low $m_T - m_0$ and thermal production at high $m_T - m_0$ [3].
 36 Kaons are fit with a m_T -Exponential function to extrapolate to low $m_T - m_0$,
 37 which assumes that enhancement effects due to Bose-Einstein statistics are
 38 mostly canceled out by suppression effects from radial flow. Proton spectra
 39 are fit with a Blast-Wave model [4] which describes the radial expansion
 40 of the fireball assuming a cylindrical expansion. By integrating the yields
 41 over the measured $m_T - m_0$ region and extrapolating to low $m_T - m_0$ the
 42 rapidity density distributions (dN/dy) are obtained.

43

3. Particle Production

44 In low energy collisions, particle production of hadrons has various dif-
 45 ferent mechanisms and can be affected by final state effects. In this section,
 46 we discuss the Coulomb potential and its effect on the pion spectra, the ratio
 47 of K^-/K^+ and its implications for different hadron production mechanisms,
 48 and measurements of baryon stopping.

49

3.1. Coulomb Potential

50 The Coulomb potential of the fireball, while small, can affect the mo-
 51 menta distributions of charged hadrons. This effect will be most evident
 52 for the charged pions as they are the lightest hadrons. Additionally, the
 53 Coulomb potential should affect positively and negatively charged pions in
 54 opposite ways: shifting π^+ to higher $m_T - m_0$ and π^- to lower $m_T - m_0$. By
 55 taking a ratio of π^+/π^- as a function of $m_T - m_0$, the Coulomb potential can
 56 be extracted using a model fit. The model incorporates the Bose-Einstein
 57 nature of pions and an effective potential to account for the momentum

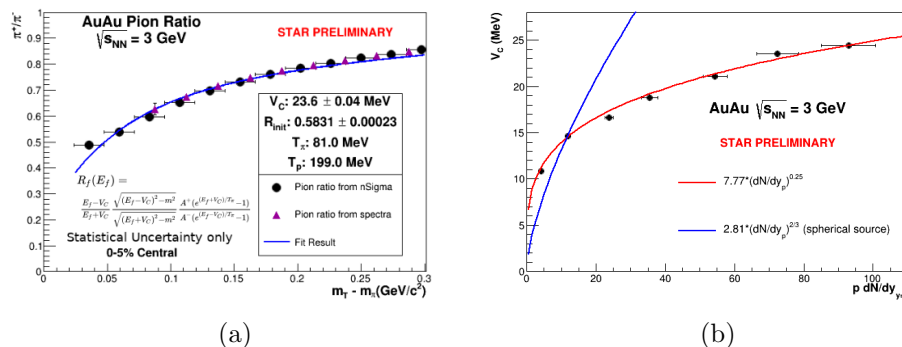


Fig. 1: (a) Ratio of π^+/π^- at midrapidity in central Au+Au collisions at $\sqrt{s_{NN}} = 3.0$ GeV. The pion ratio is fit with a model accounting for the Bose-Einstein nature of pions and an effective potential to account for the momentum distribution of stopped protons [5]. (b) Coulomb potential extracted from the pion ratio at midrapidity plotted against the midrapidity proton dN/dy for the corresponding centrality bins. Power law fits are performed with free parameters (red) and with the power fixed based on a spherical source assumption (blue), indicating the source is non-spherical.

58 distribution of stopped protons [5] (which will be discussed further in Sec.
 59 3.3). An example fit of the pion ratio with this model can be seen in Fig.
 60 1a. From this fit, the Coulomb potential (V_C) and initial pion ratio (R_{init})
 61 can be extracted. This same procedure can be applied to all centralities to
 62 obtain the Coulomb potential, which has been plotted against the midra-
 63 pidity proton dN/dy for each corresponding centrality bin in Fig. 1b. The
 64 two curves represent power law fits, following a similar study done by the
 65 HADES collaboration [6], indicating the source is non-spherical.

66 3.2. Associated Production of Kaons

67 Production of kaons is more difficult than pions due to their strangeness
 68 content. K^+ (which contain a \bar{s} quark) can be produced in association with
 69 a Λ baryon ($N + N \rightarrow N + \Lambda + K$), which is more energetically favorable
 70 compared to pair production ($N + N \rightarrow N + N + K + K$); however, both
 71 production mechanisms are available for K^+ . K^- (which contain a s quark)
 72 will not be produced via this associated mechanism as it would require the
 73 production of a $\bar{\Lambda}$, which requires much more energy; therefore, K^- are
 74 only produced in pairs with the K^+ . The ratio of K^-/K^+ indicates the
 75 fraction of K^+ that are produced in pairs with the K^- , with the remainder
 76 being produced in association with a Λ baryon. Figure 2 shows this ratio at

77 midrapidity as a function of collision energy, which follows the trend seen in
 78 previous measurements [7–11]. It also shows that approximately 5% of K^+
 79 are produced in a pair with a K^- , while the remaining 95% are produced
 80 in association with a Λ baryon at $\sqrt{s_{NN}} = 3.0$ GeV.

3.3. Baryon Stopping

81
 82 Baryon stopping
 83 occurs when par-
 84 ticipating nucleons
 85 interact with each
 86 other and lose en-
 87 ergy in the form of
 88 rapidity. Measure-
 89 ments of this ra-
 90 pidity loss provide
 91 a straight-forward way
 92 to quantify the amount
 93 of stopping. Fig-
 94 ure 3a shows the
 95 proton dN/dy distri-
 96 bution for all cen-
 97 tralities, which ex-
 98 hibits a clear trend
 99 of the peak shifting
 100 from midrapidity in
 101 central collisions to
 102 beam/target rapidity in peripheral collisions, indicating a change in the
 103 baryon stopping. Figure 3b shows the proton dN/dy in 0-5% central col-
 104 lisions, which is fit with two mirrored peaks determined by counting the
 105 number of collisions each participating nucleon takes part in a Monte-Carlo
 106 Glauber models, and smoothed using a Gaussian kernel. Stopping (δy) is
 107 defined as the shift of the projectile participant peak from beam rapidity,
 108 as demonstrated in Fig. 3b.

109
 110 The amount of stopping is obtained for all centrality classes and plotted
 111 in Fig. 4 against the average number of binary collisions divided by the aver-
 112 age number of participants divided by two ($\frac{\langle N_{Coll} \rangle}{\langle N_{part} \rangle / 2}$) for the corresponding
 113 centrality class. This can be used to estimate the average rapidity loss of
 114 a nucleon for each binary collision. In central and mid-central collisions, a
 115 clear linear trend exists which, when fit with a line, has a slope of 0.19, indi-
 116 cating that in these centrality classes, each binary nucleon-nucleon collision

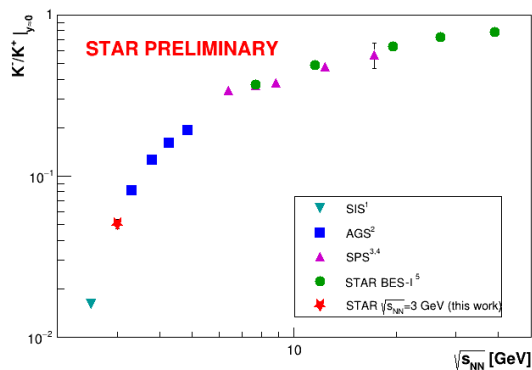


Fig. 2: Ratio of K^-/K^+ at midrapidity in central collisions. This ratio indicates the fraction of K^+ produced in pairs with a K^- , which is only about 5% at $\sqrt{s_{NN}} = 3.0$ GeV, and approaches unity for higher energy collisions. The remaining K^+ are produced in association with a Λ baryon.

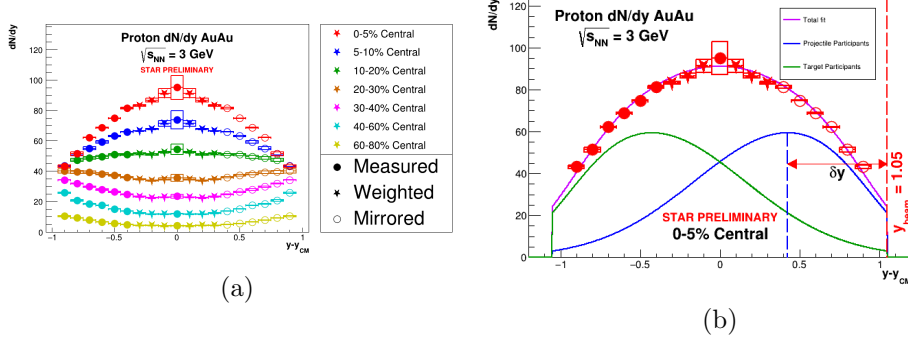


Fig. 3: (a) Proton dN/dy for all centralities. The change in shape, with the peak shifting from midrapidity toward beam/target rapidity from central to peripheral collisions, indicates a change in the baryon stopping. (b) Proton dN/dy in central collisions fit with two mirrored peaks representing the projectile (blue) and target (green) participants. The stopping, δy , is defined as the shift of the projectile participant peak from beam rapidity.

117 causes an average loss of 0.19 ± 0.01 units of rapidity. In contrast, periph-

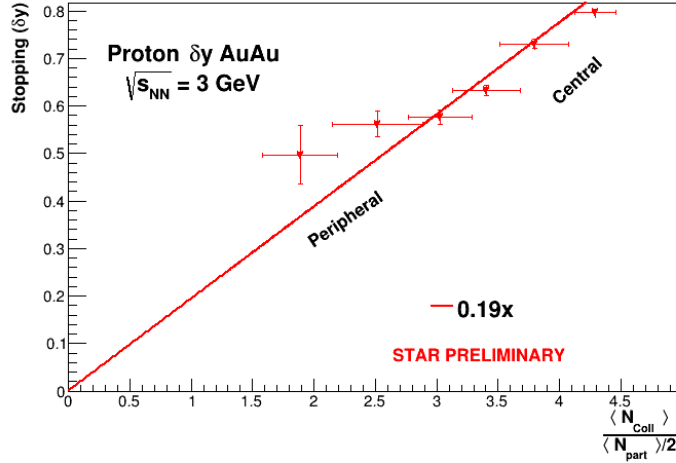


Fig. 4: Baryon stopping (δy) plotted against the average number of binary collisions per participant for all centrality classes. The linear trend in central and mid-central collisions indicates a constant average rapidity loss per binary collision of 0.19 ± 0.01 units. Peripheral collisions being above this average may indicate a larger rapidity loss from the first binary collision.

118 eral collisions fall above this linear trend, indicating each binary collision
 119 causes a larger rapidity loss. This could be explained by the first binary
 120 collision having a higher $\sqrt{s_{NN}}$ compared to successive ones, and therefore
 121 would cause a larger loss of rapidity. In these peripheral collisions where
 122 each nucleon undergoes very few binary collisions, we are perhaps seeing
 123 the larger impact of the first binary collision, which gets averaged out with
 124 more binary collisions seen in central collisions.

125 4. Summary

126 Spectra of identified π^\pm , K^\pm , and p have been measured in Au+Au
 127 Fixed-Target collisions at $\sqrt{s_{NN}} = 3.0$ GeV with STAR. The final-state
 128 Coulomb potential has been measured using the ratio of π^+/π^- , which
 129 plotted against the proton dN/dy indicates that the source of the potential
 130 is non-spherical. The ratio of K^-/K^+ has been measured and indicates
 131 that only 5% of K^+ are produced thermally in pairs with K^- , and the
 132 remaining 95% are produced in association with the Λ baryon. Finally,
 133 baryon stopping has been measured using protons and indicates that each
 134 participant has an average loss of 0.19 units of rapidity per nucleon-nucleon
 135 collision in central and mid-central collisions, whereas peripheral collisions
 136 have a higher average rapidity loss, possibly due to a larger rapidity loss
 137 from the first binary collision.

138 References

- 139 [1] STAR Collaboration. *SN0598* (2014)
 140 [2] J. Randrup and J. Cleymans. *Phys. Rev. C* 74, 047901 (2006)
 141 [3] J. L. Klay *et al.* (E895 Collaboration). *Phys. Rev. C* 68, 054905 (2003)
 142 [4] E. Schnedermann, J. Sollfrank, and U. Heinz. *Phys. Rev. C* 48, 2462–
 143 2475 (1993)
 144 [5] D. Cebra *et al.* (2014). arXiv: 1408.1369
 145 [6] J. Adamczewski-Musch *et al.* (HADES Collaboration) (2022). arXiv:
 146 2202.12750
 147 [7] Andreas Förster *et al.* (KaoS Collaboration). *Journal of Physics G:
 148 Nuclear and Particle Physics* 28.7, 2011–2015 (2002)
 149 [8] L Ahle *et al.* (E866, E917). *Phys. Lett. B* 490, 53–60 (2000)
 150 [9] C. Alt *et al.* (NA49 Collaboration). *Phys. Rev. C* 77, 024903 (2008)
 151 [10] S. V. Afanasiev *et al.* (NA49 Collaboration). *Phys. Rev. C* 66, 054902
 152 (2002)
 153 [11] L. Adamczyk *et al.* (STAR Collaboration). *Phys. Rev. C* 96, 044904
 154 (2017)